Materials Science and Engineering C 67 (2016) 65–71

Contents lists available at ScienceDirect

Materials Science and Engineering C

journal homepage: www.elsevier.com/locate/msec

Electrochemically assisted deposition of strontium modified magnesium phosphate on titanium surfaces

M. Meininger [a], C. Wolf-Brandstetter [b], J. Zerweck [a], F. Wenninger [a], U. Gbureck [a], J. Groll [a], C. Moseke [a,*]

[a] Department for Functional Materials in Medicine and Dentistry, University of Würzburg, Pleicherwall 2, D-97070 Würzburg, Germany
[b] Max Bergmann Center for Biomaterials, Technical University of Dresden, Budapester Straße 27, D-01069 Dresden, Germany

ARTICLE INFO

Article history:
Received 13 January 2016
Received in revised form 8 April 2016
Accepted 29 April 2016
Available online 04 May 2016

Keywords:
Struvite
Biomaterials
Implant
Strontium
Surface modification
Electrochemistry
Coating

ABSTRACT

Electrochemically assisted deposition was utilized to produce ceramic coatings on the basis of magnesium ammonium phosphate (struvite) on corundum-blasted titanium surfaces. By the addition of defined concentrations of strontium nitrate to the coating electrolyte Sr^{2+} ions were successfully incorporated into the struvite matrix. By variation of deposition parameters it was possible to fabricate coatings with different kinetics of Sr^{2+} into physiological media, whereas the release of therapeutically relevant strontium doses could be sustained over several weeks. Morphological and crystallographic examinations of the immersed coatings revealed that the degradation of struvite and the release of Sr^{2+} ions were accompanied by a transformation of the coating to a calcium phosphate based phase similar to low-crystalline hydroxyapatite. These findings showed that strontium doped struvite coatings may provide a promising degradable coating system for the local application of strontium or other biologically active metal ions in the implant–bone interface.

1. Introduction

Titanium has been clinically established as a reliable material for enossal implants in surgical dentistry due to its favorable mechanical and biological properties, the latter ones being a result of the highly anticorrosive passive oxide layer [1]. In order to minimize the risk of implant failure and improve the prognosis of implants even in delicate conditions of the osseous bed (e.g. osteoporosis) or in immediate loading cases, further development and modification of implant surfaces is required. The chances of early osseointegration and hence the short- and long-term stability of a titanium implant highly depend on the morphology and chemistry of its surface [2–4]. Since the 1980s calcium phosphate based ceramic materials have been deposited on implant material surfaces using plasma spray technology [5], which is up to now the most common method to combine the good biocompatibility of calcium phosphates with the excellent mechanical properties of titanium. Although the plasma spray technique has been utilized for implant applications with good results, this method has several disadvantages. Extremely high temperature gradients during the deposition of ceramics liquefied by the plasma flame induce phase changes and the formation of undesired calcium phosphate phases with different solubility [6,7]; hence, the in vivo degradation behavior of the coatings is difficult to predict [8]. An alternative coating method is electrochemically assisted deposition (ECAD), which is not a "line-of-sight" technique and can therefore be used for the homogenous coating of surfaces with complex geometries at low process temperatures. A recent study conducted in our department dealt with the electrochemical deposition of antimicrobial $Ca(OH)_2$ coatings on titanium substrates [9], with promising results regarding biocompatibility and bactericidal activity. In the present study the same ECAD setup has been adapted to magnesium and phosphate containing electrolytes to examine the possibilities for the deposition of magnesium phosphate, another promising material for bone replacement applications, which has been extensively investigated during the last years [10–15].

By the integration of biologically active trace elements into the ceramic coating further aspects of bone growth towards the metal implant surface can be positively affected. Strontium, for example, is being used in supplements for osteoporosis therapy (e.g. strontium ranelate [16, 17]). The activity of these medicaments is provided by the release of strontium ions Sr^{2+}, which stimulate the replication of pre-osteoblasts and hence support new bone formation by increased matrix synthesis on one hand and suppress bone resorption by inhibition of osteoclast activity on the other [18–23]. The incorporation of Sr^{2+} into the mineral component occurs exclusively in newly formed bone without any negative influence on its crystallographic and mechanical properties [24]. Cell-biological effects, the strength of which depends on the dosis of the Sr^{2+} ions released from a modified implant coating [25,26], will be most probably evoked in the immediate vicinity to the bone/implant interface and should be able to positively influence the osseointegration

* Corresponding author.
E-mail address: claus.moseke@fmz.uni-wuerzburg.de (C. Moseke).

http://dx.doi.org/10.1016/j.msec.2016.04.102
0928-4931/

of metal implants even in osteoporotic bone. Recently, various studies have been conducted with most promising results for the application of strontium as an agent for improved osseointegration, as well in bone replacement [27–29] as in functional coatings for implant materials [30–32]. In the study at hand, various ECAD electrolytes for the co-precipitation of the magnesium ammonium phosphate struvite ($Mg(NH_4)PO_4 \cdot H_2O$) and Sr^{2+} ions have been developed and tested; the resulting coatings were thoroughly characterized regarding their chemical and crystallographic composition, their surface morphology and their ability to release Sr^{2+} ions into physiological media. Crystallographic and topographic examinations were also carried out after immersion, in order to investigate the prognosis for the chemical transformation of the Sr-doped struvite coatings in vivo.

2. Experimental procedure

2.1. Electrochemically assisted deposition

Cathodic deposition of magnesium phosphate on corundum blasted titanium disks (cp-Ti, grade 2, Ø = 15.5mm) was carried out in a galvanostatic circuit with a single sample holder as well as with a four-sample holder and a cylindrical platinum grid serving as counter electrode. The double-walled electrochemical cell was temperature-controlled by means of a separate heating circuit. Depositions were carried out at 30 °C. The application of a constant current density was regulated by a potentiostat/galvanostat HP96 (Bank Elektronik, Pohlheim, Germany).

Titanium (cp 2) disks with 15.5 mm diameter were sandblasted with 50 μm Al_2O_3 (Korox 50, BEGO, Bremen, Germany) for 10 s at a pressure of 3 bar and a distance of 2 cm and subsequently sonicated in 5%(v/v) Extran MA 05 (Merck, Schwalbach, Germany) and twice in ultra pure water (10 min per washing step).

The ECAD electrolyte was composed of 33 mmol/L ammonium dihydrogen phosphate ($(NH_4)H_2PO_4$), 95 mmol/L HNO_3, and 50 mmol/L MgO, (all from Merck, Schwalbach, Germany). In order to find the best concentration for incorporation of strontium into the coating, strontium nitrate ($Sr(NO_3)_2$, Fluka, Munich, Germany) was added in four different amounts, 0.13 mmol/L, 1.3 mmol/L, 13 mmol/L, and 26 mmol/L.

The electrochemically assisted deposition process was conducted in a double-walled glass vessel; the electrolyte temperature was kept at 30 °C by means of a heating circulator. The pulsed ECAD current was applied using an LPG03 potentiostat/galvanostat (Bank Elektronik, Pohlheim, Germany), operated in galvanostatic mode. Current pulsing occurred with a rectangle signal (5 s current flow followed by a zero current period of 1 s), which was generated by a custom-made relay setup triggered by an Arduino UNO microcontroller (Arduino.cc, Italy). During the whole experiment the current flow was additionally controlled with a Keithley Model 2700 (Keithley, Germering, Germany). The current densities applied for the sample sets used for the Sr release studies are being provided in Table 1.

2.2. Coating characterization

The morphology of the deposited magnesium phosphate films was characterized with a field emission scanning electron microscope Crossbeam 340 (Zeiss, Oberkochen, Germany). In addition, energy dispersive X-ray spectroscopy (EDS) was performed with an INCA Energy 350 AzTec Advanced system using a silicon drift detector (SDD) (Oxford Instruments, Abingdon, UK) for the determination of coating stoichiometry and element mapping.

The crystallographic structure of the coatings was determined by X-ray diffraction (XRD) in Bragg–Brentano geometry using a Siemens D5005 X-ray diffractometer (Bruker AXS, Karlsruhe, Germany) with Cu-K_α radiation; the X-ray tube was operated at a voltage of 40 kV and a current of 40 mA. XRD patterns were recorded in a 2θ range of 10–42°, with a step size of 0.02° and a dwell time of 1 s/step.

To determine the total amount of co-deposited strontium, coatings were dissolved in HNO_3 (65%, Suprapur, Merck) and then analyzed using inductively coupled plasma mass spectroscopy (ICP-MS, Varian, Darmstadt, Germany). The device was calibrated for the determination of magnesium, phosphorus, calcium, and strontium by means of single element standard solutions (Merck, Darmstadt, Germany).

Table 1
Parameter sets for the deposition of the different coatings. For all samples the current was pulsed with $t_{on} = 5$ s and $t_{off} = 1$ s.

	Sr212	Sr290	Sr371	Sr487
Sr content in mmol/L	13	13	26	26
Current density in mA/cm²	−4.40	−3.53	−2.35	−4.40
Deposition time in min	15	25	20	15

2.3. Strontium release study

Release experiments were carried out with two different quasi-physiological media, namely simulated body fluid (SBF, composition: Na^+ 142.0 mmol/L, K^+ 5.0 mmol/L, Mg_2^+ 1.5 mmol/L, Ca_2^+ 2.5 mmol/L, Cl^- 148.8 mmol/L, HCO_3^- 4.2 mmol/L, HPO_4^{2-} 1.0 mmol/L, SO_4^{2-} 0.5-mmol/L) according to the recipe suggested by Kokubo et al. [33] without protein content on one hand, and SBF supplemented with 10% (v/v) fetal calf serum (FCS, Invitrogen Life Technologies, Karlsruhe, Germany) on the other. Each sample was immersed in 2 ml medium and stored on an orbital shaker in a warm cabinet at 37 °C. The medium was changed daily for 28 days. The liquid samples were collected and analyzed by ICP-MS to determine the concentrations of ions released from the surface into the surrounding medium.

2.4. Coating transformation study

In addition to the investigation of the strontium release kinetics, the behavior of the doped coatings during immersion in the physiological media was investigated. For this purpose, the samples used in the release experiments were thoroughly examined using XRD, SEM, and EDS, in order to determine the degree of phase transformation after 28 days. The data obtained from the measurements of the release study samples were supplemented with additional experiments of struvite immersion in cell culture medium (Dulbecco's modified Eagle's serum, DMEM, Invitrogen Life Technologies, Karlsruhe, Germany) under the same conditions as the release experiments in SBF and SBF supplemented with FCS. The variation of the immersion conditions was performed with respect to the dynamic in vivo conditions. Former experiments had shown that appropriate in vitro immersion parameters require the provision of sufficient total amounts of calcium and phosphate ions, either by frequent medium changes or increased medium volume. This was in accordance with the findings of Kokubo and Takadama [34].

3. Results and discussion

3.1. Coating characterization

In the frame of this study a huge variety of parameter sets for the co-deposition of struvite and strontium have been tested. Composition and thickness of the Sr-doped coatings could be influenced by variation of deposition time, strontium content in the electrolyte, and current density. The results of many pre-tests revealed that the strontium content could not exceed certain values, when homogeneous and dense struvite coatings were desired. In order to meet the demands of struvite coatings suitable for the functional modification of biomaterial surfaces, the parameter sets presented in this study were carefully chosen with respect to the deposition of well-defined coatings and - according to the results of pre-tests - with different strontium contents from 0.1–0.4 mg/cm², in

order to achieve daily release rates in a range from about 5 μg/cm^2 to 10 μg/cm^2.

Nevertheless, samples with big differences in the amounts of strontium addition were examined by scanning electron microscopy to investigate the crystallographic and morphological changes on the microscopic level. Fig. 1 shows SEM images of coatings deposited with different strontium additions to the standard electrolyte for struvite ECAD; the respective samples are being denominated with the molar Sr:Mg ratio in the applied electrolyte. At a low magnification of 500 the pure struvite and struvite with Sr:Mg = 0.026:1 and Sr:Mg = 0.26:1 showed quite comparable morphology and roughness (Fig. 1a–c, big images), whilst the surface of the coating with Sr:Mg = 0.51:1 in Fig. 1d revealed a rather different topography with only few well-defined crystallites, confined in a glass-like matrix with lots of microcracks. The differences became much more obvious at higher magnification of 20.000 (small inserts in Fig. 1): Pure struvite and struvite with Sr:Mg = 0.026:1 showed practically the same crystallite morphology even on the lower micrometer scale (Fig. 1a,b, small inserts). The small insert in Fig 1c reveals that in the struvite coating with Sr:Mg = 0.26:1 additional small crystallites (with a size below 100 nm) appeared on the surface of the struvite crystals. At even higher strontium addition (Sr:Mg = 0.51:1, Fig 1 d, small insert), the characteristic struvite morphology had practically vanished: the coating was dominated by extremely small crystallites; only few well-defined struvite crystallites could be observed.

X-ray diffraction patterns of the same coatings revealed quite similar findings. As can be seen in Fig. 2, the patterns of struvite and coatings deposited from electrolytes with Sr:Mg ratios 0.026:1 and 0.26:1 mainly consisted of only two phases, namely struvite itself and the underlying titanium substrate; the small additional peaks in every pattern could be attributed to corundum, a residue of the sandblasting process carried out prior to coating deposition. The integral intensity of the struvite peaks slightly decreased with rising strontium content, as compared to the Ti peaks, indicating a decreasing content of crystalline struvite in the coating. In the sample with Sr:Mg = 0.51:1, however, a dramatic reduction of the struvite peak intensities was observed. As the coatings on all examined samples had quite similar masses, this effect could not be explained by a reduced coating thickness (which was estimated to be in the range of about 2–4 μm, see Supp. 1, Fig. S1), but rather by a significant decrease of the fraction of highly crystallized struvite in the

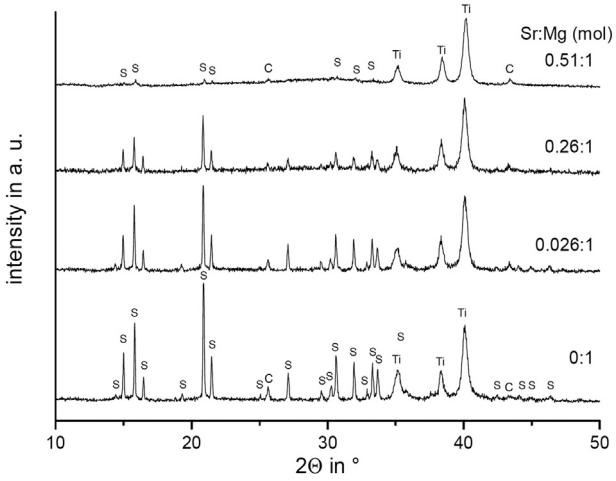

Fig. 2. X-ray diffraction patterns of struvite coatings made from electrolytes with different Sr:Mg ratios in the coating electrolyte. All samples were coated with $I = -3.75$ mA/cm^2, $t = 15$ min, and $T = 30$ °C. S = struvite, C = corundum, Ti = titanium substrate.

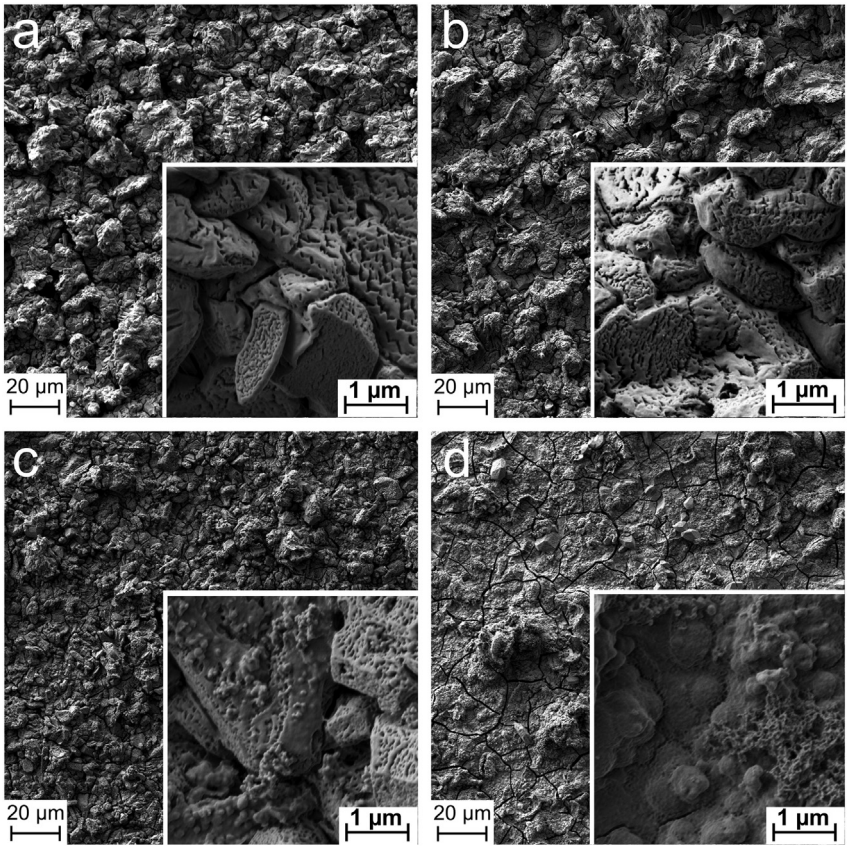

Fig. 1. Scanning electron micrographs of struvite coatings made from electrolytes with different Sr:Mg ratios in the coating electrolyte. a: 0:1, b: 0.026:1, c: 0.26:1, d: 0.51:1. All samples were coated with $I = -3.75$ mA/cm^2, $t = 15$ min, and $T = 30$ °C. Magnifications were 500× in the main images and 20.000× in the smaller inserts.

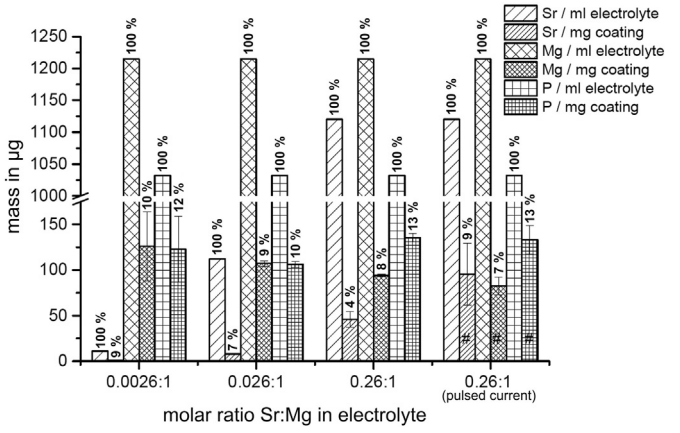

Fig. 3. Changes in coating composition in dependence on increasing strontium content in the electrolyte. All samples were coated with $I = -3.75$ mA/cm^2, $t = 15$ min, and $T = 30$ °C. Samples marked with # were coated with pulsed current ($t_{on} = 5$ s and $t_{off} = 1$ s).

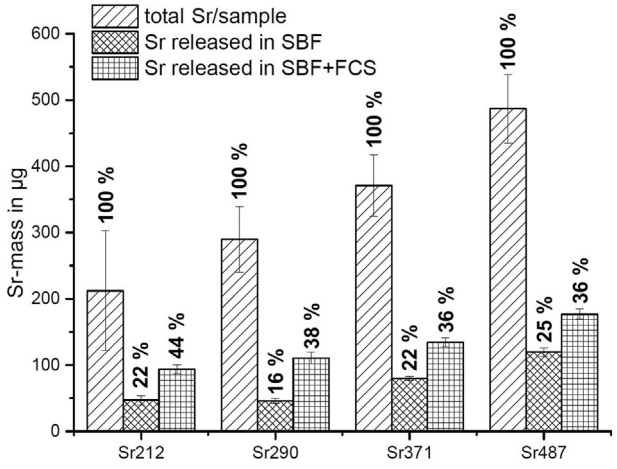

Fig. 5. Cumulated total amounts of Sr released after 28 days in SBF and SBF + 10% FCS in relation to the original Sr content (numbers on the x-axis in µg) in the examined coatings.

coatings. This assumption was supported by the observation of a small amorphous halo in the XRD pattern as well as by the application of the Scherrer equation to the peak half-widths, which led to an estimated average crystallite size reduction from about 90 nm for the pure struvite coating to 62 nm in the coating with Sr:Mg = 0.51:1 in the electrolyte. Furthermore, the XRD patterns did not reveal noticeable shifts of the peak positions; hence, with respect to the significantly different ionic radii of Mg^{2+} and Sr^{2+} (0.072 nm respectively 0.12 nm [35,36]) the incorporation of strontium ions into the struvite lattice is unlikely, as this would lead to noticeable lattice distortion. EDS analysis of the same samples showed that the molar Mg:P ratio in the undoped coating was 1.02 ± 0.01, hence practically identical to the theoretical value for struvite. With increasing Sr:Mg ratio in the electrolyte the Sr:Mg ratio in the resulting coating increased almost geometrically; with Sr:Mg = 0.51:1 in the electrolyte the coating contained even more Sr than Mg (Sr:Mg ≈ 1.58). The calculation of the molar (Mg + Sr):P ratio in this coating led to a value of 1.31, which matched exactly the theoretical value of a supposed mixture of struvite and strontium phosphate with fractions corresponding to the measured Sr and Mg fractions in the coating. As mentioned above, the respective XRD pattern showed only weak intensities of struvite peaks and no indication for the presence of any additional crystalline phase. Furthermore, EDS mapping of the sample surface showed no local concentrations, neither of magnesium nor of strontium (see Suppl. 2, Figs. S3, S4, and S5), but a very uniform spatial distribution of all elements. One possible explanation for these findings could be the presence of two different phases (struvite and strontium phosphate), each with well-defined stoichiometry, but very low crystallite size, percolating each other and forming the dense matrix, which can be seen in Fig 1d. In Fig. 1a–c representing coatings with lower Sr contents, the morphology of the bulk struvite does not reveal any significant changes. However, the brick-like and about 1 µm-sized structures represent polycrystalline agglomerates according to the crystallite size determined by the Scherrer equation. The lamellar and porous structure also allows for percolation with amorphous strontium phosphate phases, which could explain the slight decrease of the struvite peaks in the XRD patterns, while the bulk topography appears practically unchanged. The calculation of the (Mg + Sr):P ratio in the two samples with lower Sr content revealed no significant values, which would allow conclusions on the stoichiometric composition as in the sample with the highest Sr content; nevertheless the Sr distribution over the coating was also equally homogeneous, as was shown by EDS mapping. Together with the morphology revealed by SEM and the XRD patterns these findings support the assumption that the coating composition was dominated by a crystalline struvite phase, percolated by an amorphous and stoichiometrically indefinite strontium phosphate phase.

Changes in the coating composition induced by the increasing strontium content in the electrolyte are shown in Fig. 3. The values for the absolute ion content in µg per coating were calculated from the ion content in the dissolved coatings, as measured with ICP-MS; the relative values (in %) were calculated from the ratios of measured ion contents and the coating mass. In general, an increase of the strontium concentration within the electrolyte resulted in higher total strontium mass in the coatings, as more strontium was available for deposition.

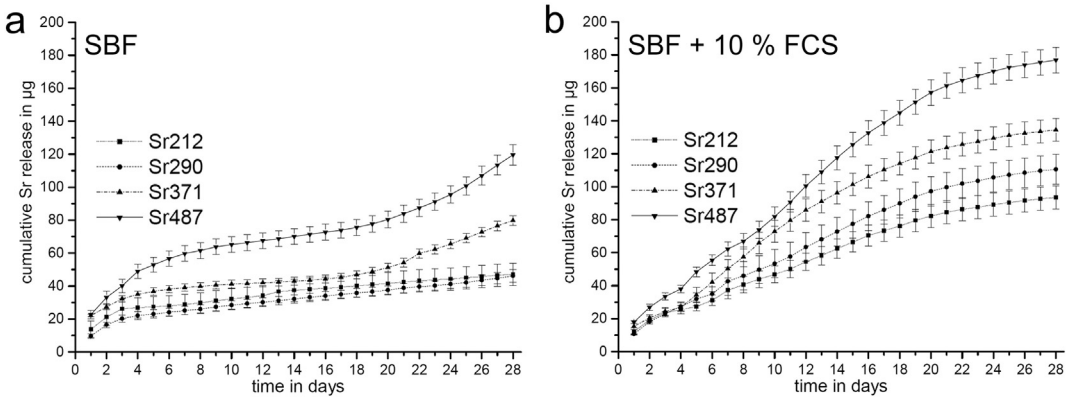

Fig. 4. Cumulated release of strontium from samples containing total amounts of 212, 290, 371, and 487 µg Sr; (a) release in synthetic body fluid, (b) release in SBF supplemented with 10% FCS.

However, the ratio of deposited strontium to the available strontium in the electrolyte decreased from 9% to 4% with an increase of the Sr:Mg ratio from 0.0026:1 to 0.26:1. Even though the Mg concentration in the electrolyte remained unchanged for all coating experiments, the deposition of increased Sr mass led to the deposition of reduced masses of Mg, which indicates that Sr was deposited as an amorphous phase of metallic Sr or strontium phosphate; these process consumed electrons and/or OH^- ions, which resulted in a reduced amount of deposited struvite.

By pulsed deposition the strontium content in coatings made from the electrolyte with a Sr:Mg ratio of 0.26:1 could be increased from 46 μg to 96 μg per mg of coating mass. Apparently, the reduced OH^- concentration during the zero current phase shifts the equilibrium to the precipitation of strontium phosphate. This assumption is supported by literature data concerning the solubility products of phosphates under various conditions [37,38], indicating that the solubility of strontium phosphate is significantly lower than that of struvite.

3.2. Strontium release study

Fig. 4 shows the cumulated release curves of struvite coated samples with strontium contents of 212, 290, 371, and 487 μg/sample during immersion in protein-free synthetic body fluid as well as in FCS-supplemented SBF. It could be observed that Sr was continuously released in both media over the whole period of 28 days. As expected, the released amounts showed a strong dependence on the total strontium amount immobilized in the coating. Furthermore, it was found that the release kinetics differed for the two immersion media, in which the experiments were carried out, which may be partially explained by the comparably differing transformation behavior of the coatings, which will be discussed in Section 3.3. In general, the release occurred with a lower rate in the protein-free SBF than in FCS-supplemented medium. In pure SBF, the release curves reached a plateau after few days for all strontium contents. For the samples containing the highest Sr amounts

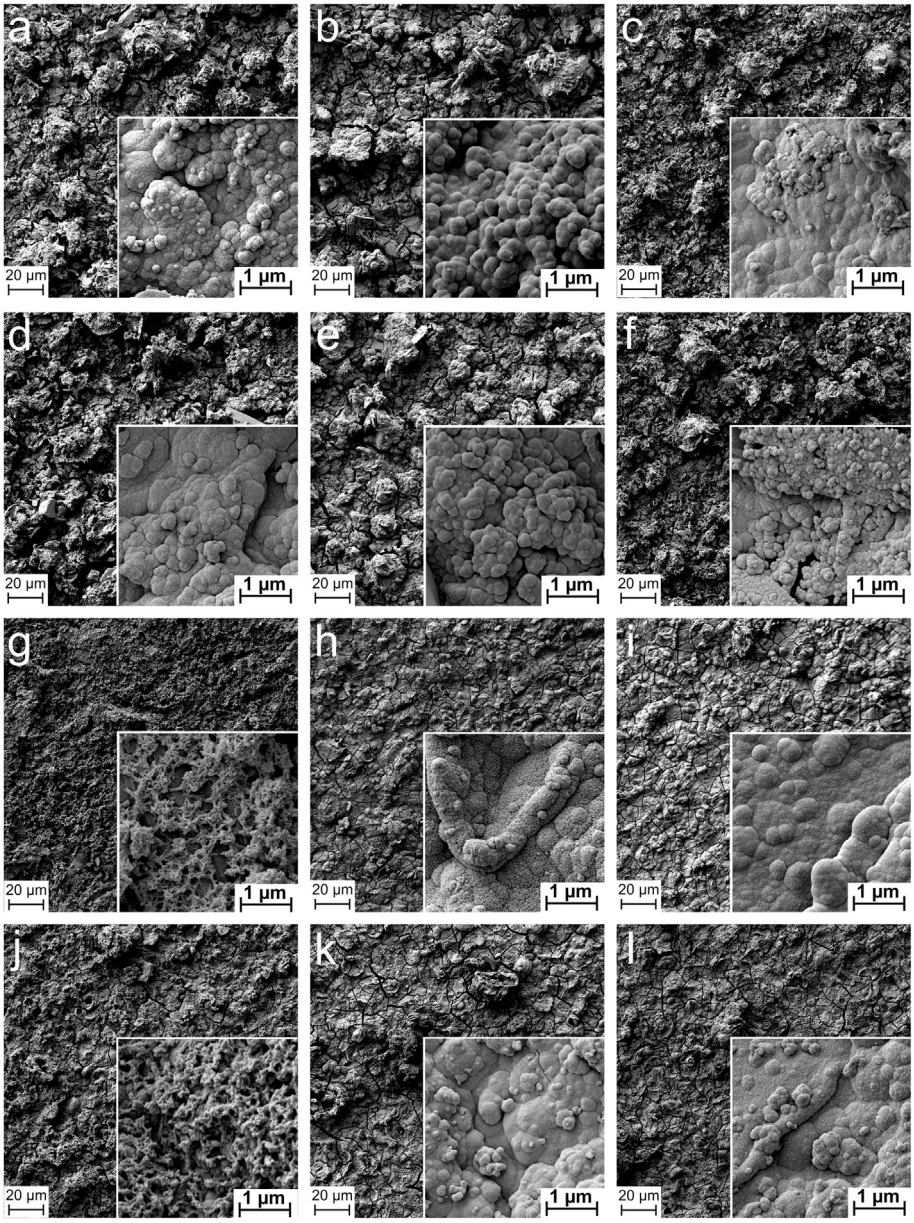

Fig. 6. Scanning electron micrographs of coatings with different Sr contents after 28 days of immersion in physiological media. Rows correspond to rising total Sr content (212, 297, 371, and 487 μg in the coating); columns correspond to immersion in SBF, SBF + FCS, and DMEM (from left to right). Magnifications were 500× in the main images and 20.000× in the smaller inserts.

(371 and 487 μg), the slopes of the cumulated release curves increased noticeably after approximately 20 days (Fig. 4a).

In FCS-supplemented SBF all release curves showed virtually constant release rates for the first 20 days; after that period the release kinetics appeared to slow down for all regarded samples (Fig. 4b). In order to investigate if this retardation occurred due to a depletion of Sr from the coatings, the initial Sr content of coatings was compared to the accumulated total amount of released Sr. The release was less than 40% in all samples and for both immersion media, which indicated a considerable amount of remaining Sr in the coating, as can be seen in Fig. 5. It should be noted that apparently the total amounts of strontium released from the different coatings during the 28 days represented practically the same fractions of the originally incorporated strontium amounts, which indicated a proportional correlation of the incorporated with the released strontium. On the one hand these findings show that the strontium release rate of the struvite coatings can be easily and reproducibly adjusted by choosing appropriate coating conditions; on the other hand, the significant contents of strontium remaining in the coatings after the release experiments support the assumption that strontium was being immobilized in the long term. It has also to be stated that the strontium release rates as well as the kinetics differed significantly between protein-free and FCS-supplemented SBF. This has to be taken into account with respect to in vivo conditions of Sr release; furthermore, extended studies will have to be conducted to fully understand the release mechanism in different physiological media, as it is apparently controlled by a complex interplay of physicochemical dissolution on one hand and coating transformation on the other.

3.3. Coating transformation study

After the release experiments a selection of samples was carefully rinsed and dried for further morphological and chemical analysis, in order to examine the changes of the coating induced by the long-term immersion in quasi-physiological environment. Fig. 6 shows SEM images of coatings from every release experiment, namely with original Sr contents of 212, 297, 371, and 487 μg and after 28 days immersion in SBF and SBF supplemented with FCS. The third column shows an additional series of samples that were immersed in DMEM under the same conditions as the samples from the release study. All samples showed mostly intact and dense coatings at optical observation. The SEM images taken at low magnification (500×) revealed similar surface topographies for the samples with original Sr amounts of 212 and 297 μg (Fig. 6a–f, big images), while the samples fabricated with the higher Sr contents of 371 and 487 μg had apparently smoother surfaces (Fig. 6g–l). On the scale of few microns all surfaces except those of samples from the SBF release study with the two highest Sr contents (see inserts in Fig. 6g and j) revealed nanostructures that differed significantly from the morphology of *as*-deposited struvite coatings, but showed high similarity to the morphological features characteristic for low-crystalline hydroxyapatite, as observed in various other studies [9,39]. This observation was supported by EDS measurements (see Supp. 3) revealing significant contents of calcium in the coatings after in-vitro transformation. In most samples the molar ratios of calcium and magnesium differed only slightly from 1; however, no apparent correlation of the Ca:Mg ratio with the strontium content and/or the immersion medium could be observed. On the other hand, the calculation of the molar ratios of the sum of magnesium, calcium, and strontium to phosphorus led to quite similar values for most samples of approximately 1.4. This would support the assumption of the presence of roughly equimolar amounts of struvite- and apatite-like phases in the converted coatings. XRD measurements (data not shown) of the same samples revealed no crystalline phases in any coating, which only allows the conclusion that these were composed of poorly crystallized phases with very low crystallite sizes. According to other immersion studies [39,40] this was explained with an inappropriate amount of provided calcium ions during the release experiments respectively with an immersion time too short for complete coating conversion. In order to further support this assumption, three samples of the coating containing an original strontium amount of 290 μg were immersed for 7 more days in the three quasi-physiological media with daily medium change. Subsequent XRD measurements of all samples revealed a characteristic bump (Fig. 7), which indicated the presence of a low-crystalline apatite-like calcium phosphate phase. The most prominent bump, however, was found in the XRD pattern of a fourth sample, consisting of pure struvite and immersed in 10 ml SBF for 10 days (see lowermost pattern in Fig. 7). SEM analysis of this sample showed the characteristic morphology of low-crystalline apatite-like calcium phosphate with the typical spherical clusters constituted of lamellar nanocrystallites (Fig. 8). EDS analysis of this coating revealed mass percentages for Ca, P, and Mg of 35.1, 17.6, and 1.2, respectively (see Suppl. 2, Fig. S6). Assuming that Mg was still present as struvite the molar Ca/P ratio could be calculated to 1.69, practically the theoretical value for hydroxyapatite. While such immersion conditions are inappropriate for the release studies due to the detection limits of the ICP-MS device, they are much

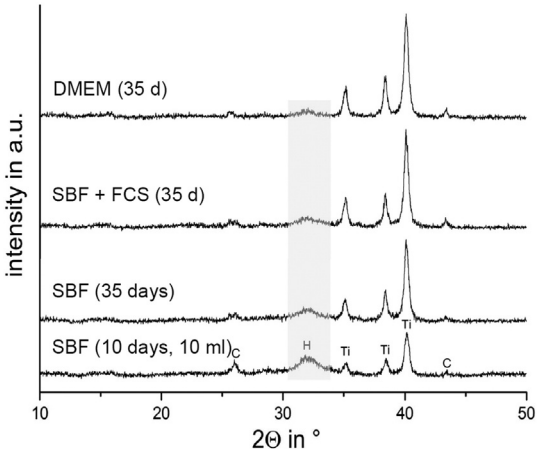

Fig. 7. X-ray diffraction patterns of selected samples after additional immersion experiments in physiological solutions. The lowermost pattern was recorded from a pure struvite coating after 10 days immersion in 10 mL SBF with daily medium change. The upper three patterns refer to coatings containing an initial total Sr amount of 290 μg after 7 days in the respective medium adding to the 28 days of the preceding release study. The shaded area corresponds to the characteristic bump of low-crystalline hydroxyapatite (H). C: corundum.

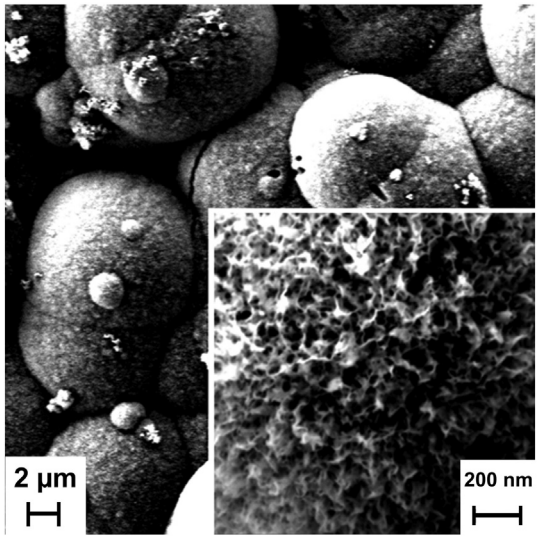

Fig. 8. Scanning electron micrograph of a struvite coated sample after 10 days immersion in 10 mL SBF with daily medium change. The insert shows the characteristic nanostructure of low-crystalline hydroxyapatite.

more representative for the in vivo conditions of constant serum flow and virtually unlimited calcium and phosphorus supplies. Hence, it may be concluded that the strontium-doped struvite coatings will – when implanted into the human body – undergo degradation and in parallel conversion to apatitic calcium phosphate with high similarity to natural bone mineral, still containing considerable amounts of strontium.

4. Conclusion

Electrochemically assisted deposition was successfully adapted to the fabrication of struvite coatings on titanium surfaces. The incorporation of defined concentrations of strontium was achieved by the modification of the coating electrolyte and the adjustment of the coating parameters, namely coating duration, current density and pulse mode. The release studies in various physiological media revealed the suitable parameter sets for the deposition of coatings that would release therapeutically relevant Sr doses for several weeks. The results of the morphological and crystallographic characterization studies before and after immersion strongly supported the assumption that the Sr-doped struvite matrix will degrade in the physiological environment and transform to a low-crystalline apatite-like phase composed of Ca as well as of residual Mg and Sr, thus constituting a highly biocompatible ceramic phase in the bone-implant interface serving as a reservoir of Sr^{2+} ions that may be released at a later time point.

Further studies, in particular extensive biological studies of osteoblast and osteoclast response to the functionalized coatings are currently conducted in order to fully explore the potential of these coatings to serve as a “smart” release system for strontium.

Acknowledgements

The authors wish to thank the Deutsche Forschungsgemeinschaft for their financial support (DFG MO 1768/2-1, WO 1903/2-1, and the DFG State Major Instrumentation Program, funding the crossbeam scanning electron microscope Zeiss CB 340 (INST 105022/58-1 FUGG)).

Appendix A. Supplementary data

Supplementary data to this article can be found online at http://dx.doi.org/10.1016/j.msec.2016.04.102.

References

[1] F.H. Jones, Teeth and bones: applications of surface science to dental materials and related biomaterials, Surf. Sci. Rep. 42 (2001) 79–205.
[2] B.D. Boyan, T.W. Hummert, D.D. Dean, Z. Schwartz, Role of material surfaces in regulating bone and cartilage cell response, Biomaterials 17 (1996) 137–146.
[3] B.-H. Lee, J.K. Kim, Y.D. Kim, K. Choi, K.H. Lee, In vivo behavior and mechanical stability of surface-modified titanium implants by plasma spray coating and chemical treatments, J. Biomed. Mater. Res. A 69A (2004) 279–285.
[4] D. Buser, R. Schenk, S. Steinemann, J. Fiorellini, C. Fox, H. Stich, Influence of surface characteristics on bone integration of titanium implants — a Histomorphometric study in miniature pigs, J. Biomed. Mater. Res. 25 (1991) 889–902.
[5] W. Suchanek, M. Yoshimura, Processing and properties of hydroxyapatite-based biomaterials for use as hard tissue replacement implants, J. Mater. Res. 13 (1998) 94–117.
[6] W. Tong, J. Chen, X. Zhang, Amorphorization and recrystallization during plasma spraying of hydroxyapatite, Biomaterials 16 (1995) 829–832.
[7] B. Koch, J. Wolke, K. Degroot, X-ray-diffraction studies on plasma-sprayed calcium phosphate-coated implants, J. Biomed. Mater. Res. 24 (1990) 655–667.
[8] R.Z. Legeros, Biodegradation and bioresorption of calcium phosphate ceramics, Clin. Mater. 14 (1993) 65–88.
[9] C. Moseke, W. Braun, A. Ewald, Electrochemically deposited Ca(OH)2 coatings as a bactericidal and osteointegrative modification of Ti implants, Adv. Eng. Mater. 11 (2009) B1–B6.
[10] C. Moseke, V. Saratsis, U. Gbureck, Injectability and mechanical properties of magnesium phosphate cements, J. Mater. Sci. Mater. Med. 22 (2011) 2591–2598.
[11] E. Vorndran, K. Wunder, C. Moseke, I. Biermann, F.A. Müller, K. Zorn, et al., Hydraulic setting Mg3(PO4)2 powders for 3D printing technology, Adv. Appl. Ceram. 110 (2011) 476–481.
[12] C. Großardt, A. Ewald, L.M. Grover, J.E. Barralet, U. Gbureck, Passive and active in vitro resorption of calcium and magnesium phosphate cements by osteoclastic cells, Tissue Eng. Part A 16 (2010) 3687–3695.
[13] R. Walter, A. Mehjabeen, T. Gordon, Mb. Kannan, Precipitation of struvite on pure magnesium and in vitro degradation behaviour, Chemeca 2013 Challenging Tomorrow 2013, p. 909.
[14] S. Meininger, S. Mandal, A. Kumar, J. Groll, B. Basu, U. Gbureck, Strength reliability and in vitro degradation of three-dimensional powder printed strontium-substituted magnesium phosphate scaffolds, Acta Biomater. 31 (2016) 401–411.
[15] Y. Liang, H. Li, J. Xu, X. Jiang, X. Li, Y. Yan, et al., Strontium coating by electrochemical deposition improves implant osseointegration in osteopenic models, Exp. Ther. Med. (2014).
[16] N. Burlet, J.-Y. Reginster, Strontium ranelate: the first dual acting treatment for postmenopausal osteoporosis, Clin. Orthop. 443 (2006) 55–60.
[17] P.J. Marie, D. Felsenberg, M.L. Brandi, How strontium ranelate, via opposite effects on bone resorption and formation, prevents osteoporosis, Osteoporos. Int. 22 (2010) 1659–1667.
[18] P.J. Marie, P. Ammann, G. Boivin, C. Rey, Mechanisms of action and therapeutic potential of strontium in bone, Calcif. Tissue Int. 69 (2001) 121–129.
[19] R. Baron, Y. Tsouderos, In vitro effects of S12911-2 on osteoclast function and bone marrow macrophage differentiation, Eur. J. Pharmacol. 450 (2002) 11–17.
[20] E. Canalis, M. Hott, P. Deloffre, Y. Tsouderos, P.J. Marie, The divalent strontium salt S12911 enhances bone cell replication and bone formation in vitro, Bone 18 (1996) 517–523.
[21] S.S. Singh, A. Roy, B. Lee, S. Parekh, P.N. Kumta, Murine osteoblastic and osteoclastic differentiation on strontium releasing hydroxyapatite forming cements, Mater. Sci. Eng. C 63 (2016) 429–438.
[22] A.S. Hurtel-Lemaire, R. Mentaverri, A. Caudrillier, F. Cournarie, A. Wattel, S. Kamel, et al., The calcium-sensing receptor is involved in strontium ranelate-induced osteoclast apoptosis — new insight into the associated signaling pathways, J. Biol. Chem. 284 (2009) 575–584.
[23] A.D. Bakker, B. Zandieh-Doulabi, J. Klein-Nulend, Strontium ranelate affects signaling from mechanically-stimulated osteocytes towards osteoclasts and osteoblasts, Bone 53 (2013) 112–119.
[24] C. Li, O. Paris, S. Siegel, P. Roschger, E.P. Paschalis, K. Klaushofer, et al., Strontium is incorporated into mineral crystals only in newly formed bone during strontium ranelate treatment, J. Bone Miner. Res. 25 (2010) 968–975.
[25] S.C. Verberckmoes, M.E. De Broe, P.C. D'Haese, Dose-dependent effects of strontium on osteoblast function and mineralization, Kidney Int. 64 (2003) 534–543.
[26] M. Grynpas, P. Marie, Effects of low-doses of strontium on bone quality and quantity in rats, Bone 11 (1990) 313–319.
[27] S. Ray, U. Thormann, U. Sommer, T. El Khassawna, M. Hundgeburth, A. Henss, et al., Effects of macroporous, strontium loaded xerogel-scaffolds on new bone formation in critical-size metaphyseal fracture defects in ovariectomized rats, Inj. Int. J. Care Inj. 47 (2016) S52–S61.
[28] U. Thormann, S. Ray, U. Sommer, T. ElKhassawna, T. Rehling, M. Hundgeburth, et al., Bone formation induced by strontium modified calcium phosphate cement in critical-size metaphyseal fracture defects in ovariectomized rats, Biomaterials 34 (2013) 8589–8598.
[29] S. Lopa, D. Mercuri, A. Colombini, G. De Conti, F. Segatti, L. Zagra, et al., Orthopedic bioactive implants: hydrogel enrichment of macroporous titanium for the delivery of mesenchymal stem cells and strontium, J. Biomed. Mater. Res. A 101 (2013) 3396–3403.
[30] V. Offermanns, O.Z. Andersen, G. Falkensammer, I.H. Andersen, K.P. Almtoft, S. Sorensen, et al., Enhanced osseointegration of endosseous implants by predictable sustained release properties of strontium, J. Biomed. Mater. Res. B Appl. Biomater. 103 (2015) 1099–1106.
[31] Y. Liang, H. Li, J. Xu, X. Li, M. Qi, M. Hu, Morphology, composition, and bioactivity of strontium-doped brushite coatings deposited on titanium implants via electrochemical deposition, Int. J. Mol. Sci. 15 (2014) 9952–9962.
[32] M.J. Frank, M.S. Walter, H. Tiainen, M. Rubert, M. Monjo, S.P. Lyngstadaas, et al., Coating of metal implant materials with strontium, J. Mater. Sci. Mater. Med. 24 (2013) 2537–2548.
[33] T. Kokubo, H. Kushitani, S. Sakka, T. Kitsugi, T. Yamamuro, Solutions able to reproduce Invivo surface-structure changes in bioactive glass-ceramic a-W3, J. Biomed. Mater. Res. 24 (1990) 721–734.
[34] T. Kokubo, H. Takadama, How useful is SBF in predicting in vivo bone bioactivity? Biomaterials 27 (2006) 2907–2915.
[35] R. Yu, X. Wang, Y. Fu, L. Wang, S. Cai, M. Liu, et al., Effect of magnesium doping on properties of lithium-rich layered oxide cathodes based on a one-step co-precipitation strategy, J. Mater. Chem. A 4 (2016) 4941–4951.
[36] H. Shi, F. He, J. Ye, Synthesis and structure of iron- and strontium-substituted octacalcium phosphate: effects of ionic charge and radius, J. Mater. Chem. B 4 (2016) 1712–1719.
[37] L.E. Holt, J.A. Pierce, C.N. Kajdi, The solubility of the phosphates of strontium, barium, and magnesium and their relation to the problem of calcification, J. Colloid Sci. 9 (1954) 409–426.
[38] J.D. Doyle, S.A. Parsons, Struvite formation, control and recovery, Water Res. 36 (2002) 3925–3940.
[39] L. Jonášová, F.A. Müller, A. Helebrant, J. Strnad, P. Greil, Biomimetic apatite formation on chemically treated titanium, Biomaterials 25 (2004) 1187–1194.
[40] S. Ban, S. Maruno, Morphology and microstructure of electrochemically deposited calcium phosphates in a modified simulated body fluid, Biomaterials 19 (1998) 1245–1253.